Available online at www.sciencedirect.com
SCIENCE DIRECT
Dyes and Pigments 72 (2007) 357–362
DYES and PIGMENTS
www.elsevier.com/locate/dyepig

Theoretical study on the structures and absorption properties of styryl dyes with quinoline nucleus

Lan-Ying Wang [a,*], Qin-Wen Chen [a], Gao-Hong Zhai [a], Zhen-Yi Wen [b], Zu-Xun Zhang [a]

[a] *Department of Chemistry, Northwest University, Xi'an 710069, China*
[b] *Institute of Modern Physics, Northwest University, Xi'an 710069, China*

Received 10 May 2005; received in revised form 12 July 2005; accepted 12 September 2005
Available online 10 November 2005

Abstract

The ground-state geometries, the lowest energy transitions and the electronic spectra for a series of styryl dyes with quinoline nucleus have been studied with TD-DFT including SCRF approach. TD-DFT calculations provide a correct description of the UV–Vis spectra of these dye molecules. Moreover, the $\pi \rightarrow \pi^*$ type absorption bands of unsubstituted or substituted styrylquinolines are all reasonably well reproduced by TD-DFT at the B3LYP/6-311G** level. Compared with our previously reported experimental data, the average relative deviation of λ_{max} is −2.56% in gas phase and −2.48% in methanol solvent.

Keywords: Styryl dyes with quinoline nucleus; TD-DFT; SCRF; Transition energy; UV–Vis spectrum

1. Introduction

The styryl dyes with quinoline nucleus are among the most widely used class of organic functional dyes. They were synthesized and applied to various sensitive materials such as sensitizers or desensitizers formerly [1]. With the development of relative technology, people developed the application of styrylquinoline dyes to electroluminescence and photochromism [2–4], as well as the field of medication [5–8]. Our previous efforts have been devoted to develop the synthesis and applications of cyanine and styryl dyes [9–13]. There are many literatures on the synthesis and applications of styryl dyes with quinoline. However, few structures and absorption properties of styrylquinoline dyes have been calculated as test cases so far.

Density functional theory (DFT), as an approximation method for ab initio calculation of electronic structures of many-particle systems, is one of the most successful and widely used methods in the computational quantum chemistry, which can be a powerful theoretical tool in the design of dyes and has already played an important role. In recent years, DFT has also been extended to excited states, and time-dependent density functional theory (TD-DFT) calculations of excited states of large organic molecules [14,15] and the chromophoric properties of organic dyes [16,17] have been made accessible for practical applications.

In this paper, we set out to explore the electronic structures of styryl dyes with quinoline nucleus using TD-DFT methods, and gave a comprehensive analysis of the effects of *p*-substituting groups (Cl, CH_3, OH, OCH_3, $N(CH_3)_2$) and *m*-substituting group (NO_2) on the ground-state geometries, energies of frontier molecular orbitals and absorption wavelengths, and also paid attention to the influence of solvent effects [18] on the electronic spectra by means of the self-consistent reaction field (SCRF) method [19,20]. The goal of this theoretical study is to elucidate the modifications in the electronic structure and to predict the changes of λ_{max} in the ultraviolet and visible regions of styryl dyes with quinoline nucleus. This could be helpful in the devise and syntheses of new dye molecules.

* Corresponding author. Tel.: +86 29 88303403; fax: +86 29 88303798.
E-mail address: wanglany@nwu.edu.cn (L.-Y. Wang).

0143-7208/$ - see front matter © 2005 Elsevier Ltd. All rights reserved.
doi:10.1016/j.dyepig.2005.09.017

2. Details of calculation

DFT calculations were carried out using Becke's three-parameter exchange function (B3) [21] and the Lee–Yang–Parr correlation function (LYP) [22]. Initial searching of steady ground-state (S_0) structures of seven different styryl dyes with quinoline nucleus was carried out by geometry optimization with the 6-31G basis set without any symmetry constraint. The obtained structures were adapted with suitable symmetry constraint and then used for the final optimization using 6-31G, 6-31G* and 6-311G** basis sets. Analytic frequency calculations were done to confirm that the optimized structures were of minimum energy. Calculations of the vertical excitation energies and oscillator strengths in low-lying singlet excited states were carried out at the three equilibrium geometries using TD-DFT method. Typically, according to the Franck–Condon principle, the maximum absorption peak (λ_{max}) in an UV–Vis spectrum correspond to vertical excitation.

In addition, we have also investigated solvent effects on the dye molecules. The molecular volume was calculated to estimate the cavity radius a_0 for the Onsager SCRF model at the B3LYP /6-311G** level, the SCRF geometry optimization began at the optimized gas phase structure, and the SCRF frequencies were calculated at the SCRF optimized structure. All calculations reported in this work were carried out with the Gaussian 98 program [23] and the experimental data from our previous work are listed in order to determine the most appropriate quantum chemical approach for this dye system.

3. Results and discussion

3.1. Geometric structures and symmetries

To obtain the most stable ground-state (S_0) geometries, the three different basis sets, 6-31G, 6-31G* and 6-311G**, were used for the calculations of seven styryl dyes with quinoline nucleus. The structures obtained from B3LYP/6-311G** calculations are given in Fig. 1. From Fig. 1, we can see that the molecular frameworks of these dyes are mostly constrained to be planar and the respective substitution by *m*-NO_2, *p*-Cl, *p*-OH, *p*-CH_3, *p*-OCH_3 or *p*-$N(CH_3)_2$ does not distort the carbon skeleton which remains essentially planar. Remark that we preferred to carry out electronic structure calculations of substituted dye molecules under C_s to make comparison easier with respect to unsubstituted one.

It is unclear which method is better for determining the ground-state structure at this stage, since there is no experimental structure observed. Therefore, we have calculated the maximum absorption peaks (λ_{max}) at B3LYP geometries, which can be compared with experimental data.

3.2. Transition energies

The frontier molecular orbitals of styrylquinoline dyes are recorded in Table 1. We notice in Table 1 that except HOMO − 2 having symmetry a', all the frontier orbitals listed have symmetry a''. Further investigation on the styrylquinoline derivatives with the effect of substitution indicates that both the energies of HOMO and LUMO are increased when the substituent is an electron donor group, and decreased when the substituent is an electron acceptor group. The energy sequences of HOMO and LUMO are all **a** < **b** < **c** < **d** < **e** < **f** < **g**. The reason suggested here is that electron-withdrawing substituents (Cl and NO_2) on terminal benzene ring decrease the electron density on the large conjugated-system, and electron-donating substituents (CH_3, OH, OCH_3, $N(CH_3)_2$) on C-16 position increase the π electron density. The larger the electron-donating ability of the substituent, the larger the electron density on the large conjugated-system (Table 2). However, both electron donor and electron acceptor substituents are effective in reducing the energy gap between HOMO and LUMO in the *para*-, or *meta*-substituted styryl dyes with quinoline nucleus. According to the electronic structure analysis, the orbital energy of LUMO decreases more than that of HOMO in the dyes **a** and **b**, and the energy gap of HOMO − LUMO decreases in the styrylquinoline dyes. In contrast, the orbital energy of HOMO increases more than that of LUMO in the dyes **d**, **e**, **f** and **g**, therefore the energy gap of HOMO − LUMO also decreases in the styrylquinoline dyes. These results are meaningful, because the energy gaps of frontier orbitals are related to the electron excitation. The details of calculations and analyses for absorption spectra are given in the next section.

3.3. UV–Vis absorption spectra

Table 3 lists the data of the experimental and calculated λ_{max} (nm) for the lower-lying singlet excited states of seven styrylquinoline dyes. In addition, we applied the Onsager model of TD-DFT/SCRF at B3LYP/6-311G** level to these dye molecules in order to explore the effects of solvent on absorption spectra and to test the theoretical approach against the available experimental results.

3.3.1. Comparison of the observed and calculated absorption spectra

The 6-311G** results deviate in the range from 1 to 17 nm from the experimental values and the average relative deviation is −2.56% in the gas phase and −2.48% in the methanol solvent, that is, both TD-DFT and TD-DFT/SCRF can reproduce experimental results in these dye molecules reasonably well. The 6-311G**'s results are more close to experimental data than the 6-31G's except for dye **g**, but the discrepancy is so little that we prefer to choose the former to predict the electronic excitation spectra of these dye molecules.

Furthermore, considering that the introduction of a solvent reaction field has little effect on the UV–Vis spectra of styryl dyes with quinoline nucleus, theoretical absorption wavelengths (not including SCRF effect) are plotted against the experimental ones based on three basis levels in Fig. 2.

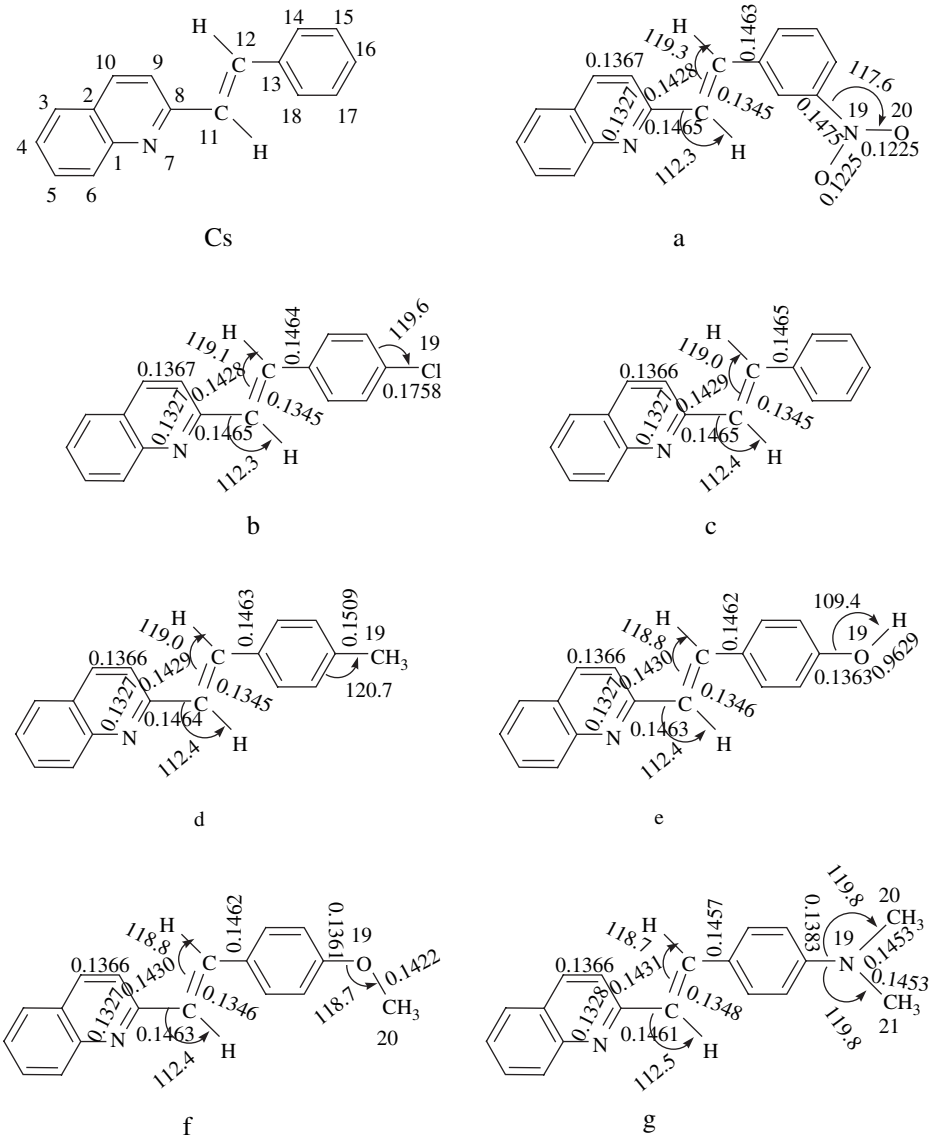

Fig. 1. Selected bond lengths (nm) and bond angles (°) of dyes according to the B3LYP/6-311G** level.

The maximum of absolute deviation between experimental and calculated λ_{max} (highest oscillator strength) from linear plot amounts for $\pi \rightarrow \pi^*$ transitions is 17 nm at 6-311G** level and 21 nm at 6-31G level. Anyhow, overall the outcomes are quite satisfactory.

3.3.2. The effect of substitution on absorption spectra

From Table 3, it could also be found that the sequence of λ_{max} is **a** < **c** < **b** < **d** < **e** < **f** < **g**, which is basically consistent with our previously reported experimental results [11]. The sequence of corresponding excitation energy is

Table 1
Orbital energies (eV) for the seven styrylquinoline dyes at B3LYP/6-311G** level

	a	**b**	**c**	**d**	**e**	**f**	**g**
LUMO + 3	−0.72(15*a*″)	−0.43(15*a*″)	−0.22(13*a*″)	−0.18(14*a*″)	−0.07(14*a*″)	−0.03(15*a*″)	0.12(16*a*″)
LUMO + 2	−1.54(14*a*″)	−0.075(14*a*″)	−0.39(12*a*″)	−0.36(13*a*″)	−0.50(13*a*″)	−0.42(14*a*″)	−0.22(15*a*″)
LUMO + 1	−2.35(13*a*″)	−1.40(13*a*″)	−1.27(11*a*″)	−1.22(12*a*″)	−1.18(12*a*″)	−1.16(13*a*″)	−1.01(14*a*″)
LUMO	−2.60(12*a*″)	−2.17(12*a*″)	−2.00(10*a*″)	−1.94(11*a*″)	−1.87(11*a*″)	−1.85(12*a*″)	−1.67(13*a*″)
HOMO	−6.33(11*a*″)	−6.04(11*a*″)	−5.93(9*a*″)	−5.80(10*a*″)	−5.64(10*a*″)	−5.58(11*a*″)	−5.08(12*a*″)
HOMO − 1	−6.81(10*a*″)	−6.68(10*a*″)	−6.58(8*a*″)	−6.53(9*a*″)	−6.49(9*a*″)	−6.46(10*a*″)	−6.25(11*a*″)
HOMO − 2	−7.33(61*a*′)	−7.21(58*a*′)	−7.09(52*a*′)	−7.04(55*a*′)	−6.96(55*a*′)	−6.89(58*a*′)	−6.51(61*a*′)
HOMO − 3	−7.64(9*a*″)	−7.28(9*a*″)	−7.13(7*a*″)	−7.07(8*a*″)	−7.00(8*a*″)	−6.98(9*a*″)	−6.83(10*a*″)
E^a	3.73	3.87	3.93	3.86	3.77	3.73	3.41

[a] The HOMO − LUMO energy gap.

Table 2
Net charge population of seven styrylquinoline dyes at B3LYP/6-311G** level

	N_7	C_8	C_{11}	C_{12}	C_{14}	C_{16}	N/Cl/C/O_{19}	O/C_{20}
a	−0.3543	0.0916	−0.0730	−0.0598	−0.0467	−0.0397	0.1774	−0.2665
b	−0.3584	0.0957	−0.0811	−0.0564	−0.0744	−0.2371	−0.0685	–
c	−0.3588	0.0964	−0.0818	−0.0580	−0.0751	−0.0832	–	–
d	−0.3595	0.0967	−0.0846	−0.0570	−0.0739	−0.0970	−0.2561	–
e	−0.3604	0.0974	−0.0890	−0.0542	−0.0739	0.1576	–	−0.3557
f	−0.3611	0.0977	−0.0895	−0.0533	−0.0719	0.1797	−0.3452	−0.1332
g	−0.3625	0.0982	−0.0942	−0.0527	−0.0821	0.2661	−0.4657	−0.1648

Table 3
Computed λ_{max} (nm) with parenthesized oscillator strength (f) for the lower-lying singlet excited states of dyes

Dyes	Calculated[a]				Exptl. in MeOH[c]
	Gas phase			Solution[b]	
	6-31G geometry	6-31G* geometry	6-311G** geometry	6-311G** geometry	
a	324.66 (0.9190)	327.28 (0.7009)	331.33 (0.8849)	331.53 (0.8711)	337.0
b	331.15 (1.0526)	336.62 (1.0993)	339.20 (1.1253)	338.99 (1.1080)	353.0
c	330.60 (0.8022)	332.76 (0.8668)	334.76 (0.1055)	334.85 (0.8934)	352.0
d	337.24 (0.8768)	338.80 (0.9462)	341.08 (0.9644)	341.14 (0.9703)	355.0
e	345.05 (0.8282)	347.61 (0.8632)	349.62 (0.8732)	350.10 (0.8913)	355.5
f	351.00 (0.8752)	352.32 (0.9175)	354.96 (0.9299)	355.32 (0.9449)	356.0
g	391.45 (0.8517)	385.64 (0.9247)	389.42 (0.9367)	390.41 (0.9552)	396.0
% A.R.D.[d]	−3.77	−3.33	−2.56	−2.48	–

[a] B3LYP function is used.
[b] Solvent ($\varepsilon = 32.63$) is methanol.
[c] Ref. [11].
[d] Average relative deviation.

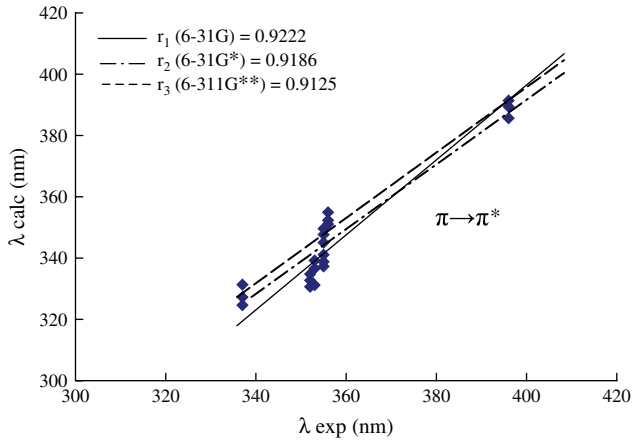

Fig. 2. Linear correlation between experimental and theoretical wavelength of $\pi \rightarrow \pi^*$ transition calculated by TD-DFT.

g < **f** < **e** < **d** < **b** < **c** < **a** (Table 4). The reason for the effect of substitution on absorption spectra suggested here is that the electron-donating substituents on C-16 position increase the electron density on the large conjugated-system. Meantime, the chlorine, oxygen, nitrogen or σ-bond of carbon–hydrogen of CH_3 joins the conjugated-system, which makes the conjugated-system become larger. Both effects of electron-donating substituents on the contraposition of benzene ring make band-gap of the conjugated-system lower, that is, the energy from HOMO to LUMO becomes smaller. Electron-withdrawing substituent on C-17 position makes band-gap obviously increased, such as dye **a**. Therefore, electron-donating substituent makes molecular λ_{max} longer. The electron-donating ability of substituents is $N(CH_3)_2 > OCH_3 > OH > CH_3 > Cl > H$, leading to the sequence of λ_{max} **g** > **f** > **e** > **d** > **b** > **c** > **a**.

Table 4
Main orbital compositions of the computed lower-lying singlet excited states of dyes at 6-311G** basis

	State	Main contribution	Transition character[a]	Excitation energy[b]	Transition feature
a	$^1A'$	$11a'' \rightarrow 12a''$	HOMO → LUMO (0.66318)	3.2551 (0.0222)	$\pi \rightarrow \pi^*$
	$^1A'$	$11a'' \rightarrow 13a''$	HOMO → LUMO + 1 (0.59550)	3.7420 (0.8849)	$\pi \rightarrow \pi^*$
b	$^1A'$	$11a'' \rightarrow 12a''$	HOMO → LUMO (0.62147)	3.6552 (1.1253)	$\pi \rightarrow \pi^*$
c	$^1A'$	$9a'' \rightarrow 10a''$	HOMO → LUMO (0.56075)	3.7036 (0.1055)	$\pi \rightarrow \pi^*$
d	$^1A'$	$10a'' \rightarrow 11a''$	HOMO → LUMO (0.61230)	3.6350 (0.9644)	$\pi \rightarrow \pi^*$
e	$^1A'$	$10a'' \rightarrow 11a''$	HOMO → LUMO (0.61667)	3.5462 (0.8732)	$\pi \rightarrow \pi^*$
f	$^1A'$	$11a'' \rightarrow 12a''$	HOMO → LUMO (0.62582)	3.4929 (0.9299)	$\pi \rightarrow \pi^*$
g	$^1A'$	$12a'' \rightarrow 13a''$	HOMO → LUMO (0.64156)	3.1838 (0.9367)	$\pi \rightarrow \pi^*$

[a] Configuration coefficients are given in parenthesis.
[b] Oscillator strengths (f) are given in parenthesis.

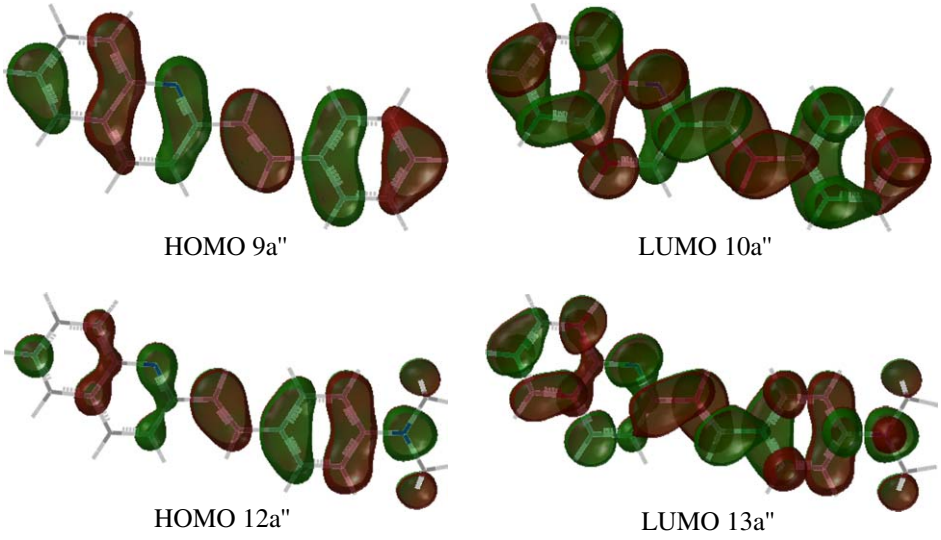

Fig. 3. Molecular orbitals of dye **c** (upper half) and dye **g** (lower half).

3.3.3. Assignment of the calculated transition

Table 4 lists the main orbital compositions of the computed lower-lying singlet excited states and transition feature of the dye molecules obtained by TD-DFT calculations. It has been found that the lowest energy absorption in dyes is due to the electronic $\pi \rightarrow \pi^*$ transition from HOMO to LUMO except for dye **a**, so it is necessary to examine the frontier orbitals of dye **a** and to interpret the influence of the substituted nitryl group. The frontier orbitals of dyes **b**, **d**, **e**, **f** and **g** are very similar to that of dye **c**. For instance, the molecular orbitals of the HOMO and LUMO for dyes **c** and **g** are depicted in Fig. 3.

The first main transitions were observed by the coefficient of HOMO → LUMO excitation when gradually replacing H by Cl, OH, CH_3, OCH_3 or N $(CH_3)_2$ to C-16 position. However, when the nitryl is attached to C-17 position of styrylquinoline dye molecule, the transition character is changed. In the first transition, the main absorption corresponding to transition from HOMO ($11a''$) to LUMO ($12a''$) in dye **a** is observed, but the oscillator strength (f) is just 0.0222, and the excitation energy corresponding to the absorption maximum is 3.2551 eV (381 nm), which is more than 44 nm of the value found in the experimental data of dye **a**. The second transition occurring at 3.7420 eV (331 nm) is an excitation from the HOMO ($11a''$) to the LUMO + 1 ($13a''$), which is in good agreement with experimental value, with the deviation from the experimental data being 6 nm for TD-B3LYP (6-311G basis) calculation. According to these calculations of dye **a**, the orbitals involved in the two lowest energy transitions are presented in Fig. 4.

Take the dyes **c** and **g**, for example, the longest absorption band is a transition mainly from HOMO to LUMO, which are all localized in the whole carbon skeleton (Fig. 3). It has been found that the electronic $\pi \rightarrow \pi^*$ transitions in styrylquinoline dye molecules are localized in the main molecular skeleton. However, the HOMO of dye **a** (Fig. 4), is mainly distributed at styrylquinoline fragment, the same as LUMO + 1, which is obviously different from LUMO. That is why the longest absorption band of dye **a** is a charge transfer transition not from HOMO to LUMO but from HOMO to LUMO + 1, and the assigned $\pi \rightarrow \pi^*$ transition which is localized in the main molecular skeleton is also confirmed. The calculation outcomes are in good agreement with experimental data, and accurately explain the experimental results.

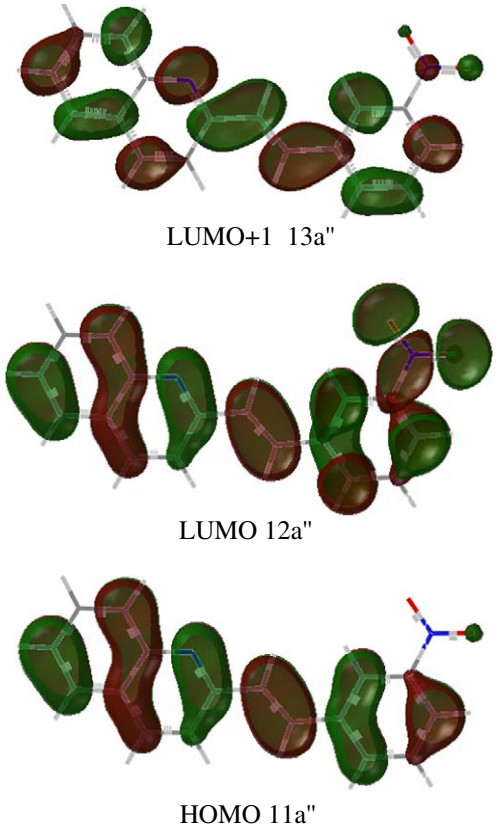

Fig. 4. Molecular orbitals of dye **a**.

4. Conclusions

The TD-DFT approach, including using Onsager model has been applied to the study of the UV–Vis spectrum of styryl dyes with quinoline nucleus for the first time. The maximum absorption wavelengths (λ_{max}) are in very good agreement with the reported absorption spectrum. These results suggest that TD-DFT methods can be used for the prediction of the excitation spectra, particularly the excitation energy for the lowest energy transition corresponding to the λ_{max}. In addition, the calculations show correctly that *p*-substituents (Cl, CH_3, OH, OCH_3, $N(CH_3)_2$) and *m*-substituent (NO_2) at the end benzene ring result in red-shift and blue-shift for $\pi \rightarrow \pi^*$ type absorption band, respectively, confirming the intramolecular nature of the absorption transition.

In summary, TD-DFT appears as a valuable general method in the calculation of the excitation of styryl dyes with quinoline nucleus, which will attract a lot of attention that would help us to investigate and design the optical behaviors of the planar-conjugated dye molecules, even nonplanar ones.

Acknowledgements

We appreciate the financial support for this research by a grant from the Special Science Research Foundation of Education Committee (No. 02JK060) and the Natural Science Foundation of Shaanxi Province (No. 2004B23).

Reference

[1] Hamer FM. The cyanine dyes and related compound. New York: Interscience Publishers; 1964.
[2] Makoto M, Hisato T, Hiromitsu T, Osamu W, Tomohiko M, Seiji T. Jpn Kokai Tokkyo Koho Jpn 2000;260:566 [Chem Abstr 2000, 133, 244894].
[3] Lap Kin C, Lap-Tak Andrew C. Eur Pat Appl EP 1 107 063; 2001 [Chem Abstr 2001, 135, 26878].
[4] Spalletti A. Conformer-specific and two-fold adiabatic photoisomerization of *ZZ*-1,4-di-(2-quinolylethenyl) benzene. Photochem Photobiol Sci 2004;3(7):695–9.
[5] Maguire MP, Sheets KR, Mcvety K, Spada AP, Zilberstein A. A new series of PDGF receptor tyrosine kinase inhibitors: 3-substituted quinoline derivatives. J Med Chem 1994;37(14):2129–37.
[6] Orme MW, Baindur N, Robbins KG, Harris SM, Kontoyianni M, Hurley LH, et al. PCT Int Appl, WO 98 17,267; 1998 [Chem Abstr 1998, 128, 321662].
[7] Mousnier A, Leh H, Mouscadet JF, Dargemont C. Nuclear import of HIV-1 integrase is inhibited in vitro by styrylquinoline derivatives. Mol Pharmacol 2004;66(4):783–8.
[8] Bonnenfant S, Thomas CM, Vita C, Subra F, Deprez E, Zouhiri F, et al. Styrylquinolines, integrase inhibitors acting prior to integration: a new mechanism of action for anti-integrase agents. J Virol 2004;78(11): 5728–36.
[9] Zhang ZX, Zhang YJ, Hao JX, Zhang ZJ, Li CE. Synthesis of a new silacarbocyanine dye and its application in silver bromide emulsion. Sci China (Ser B) 1995;25(7):689–93.
[10] Zhang CL, Wang LY, Zhang XH, Zhang ZX, Cao ZX. Studies of photosensitive dyes binding to monocrystalline germanium surface. J Funct Mater 2001;32(5):546–7, 550.
[11] Li FM, Wang LY, Wang SHK, Zhang ZX. Solvent-free rapid synthesis of styryl dyes with quinoline nucleus using microwave irradiation. J Org Chem 2004;24(1):50–2.
[12] Wang LY, Zhang XG, Shi YP, Zhang ZX. Microwave-assisted solvent-free synthesis of some hemicyanine dyes. Dyes Pigments 2004; 62(1):21–5.
[13] Wang LY, Zhang XG, Li FM, Zhang ZX. Microware-assisted solvent-free synthesis of some styryl dyes with benzimidazole nucleus. Synth Commun 2004;34(12):2245–52.
[14] van Gisber SJA, Snijders JG, Baerends EJ. Time-dependent density functional results for the dynamic hyperpolarizability of C_{60}. Phys Rev lett 1997;78(16):3097–100.
[15] Bauernschmitt R, Ahlrichs R, Hennrich FH, Kappes MM. Experiment versus time density functional theory prediction of fullerene electronic absorption. J Am Chem Soc 1998;120(20):5052–9.
[16] Dominique G, Shinichiro N. Calculation of the absorption wavelength of dyes using time-dependent density-functional theory (TD-DFT). Dyes Pigments 2000;46(2):85–92.
[17] Seiji I, Hiroo F, Hidetoshi K, Makoto I, Nobuaki K. Theoretical study on the structures and absorption properties of yellow azomethine dyes. Bull Chem Soc Jpn 2003;76(4):733–42.
[18] Tomasi J, Persico M. Molecular interactions in solution: an overview of methods based on continuous distribution of the solvent. Chem Rev 1994;94(7):2027–94.
[19] Onsager L. Electric moments of molecules in liquids. J Am Chem Soc 1936;58:1486–93.
[20] Wong MW, Frisch MJ, Wiberg KB. Solvent effects. 1. The mediation of electrostatic effects by solvents. J Am Chem Soc 1991;113(13):4776–82.
[21] Becke AD. Density-functional thermochemistry. III. The role of exact exchange. J Phys Chem 1993;98(7):5648–52.
[22] Lee C, Yang W, Parr RG. Development of the Colle–Salvetti correlation-energy formula into a functional of the electron density. Phys Rev B 1988;37(2):785–9.
[23] Frisch MJ, Trucks GW, Schlegel HB, Scuseria GE, Robb MA, Cheesemann JR, et al. Gaussian 98, revision A.6. Pittsburgh, PA: Gaussian, Inc.; 1998.